# New techniques for predicting the multipath fading distribution on VHF/UHF/SHF terrestrial line-of-sight links in Canada

# Méthodes nouvelles pour la prédiction de la distribution de l'affaiblissement multivoie sur les liaisons terrestres VHF/UHF/SHF en ligne de vue au Canada

R.L. Olsen *and* B. Segal, *Communications Research Centre, Department of Communications, P.O. Box 11490, Station H, Ottawa, Ont. K2H 8S2*

New methods are presented for predicting the signal fading distribution due to multipath propagation for the average worst month on VHF/UHF/SHF terrestrial line-of-sight links in Canada. One method for the deep fading range does not require detailed path profile information and is designed for preliminary planning or licensing purposes. A second method which does employ the path profile is intended for more detailed design purposes. A third method, complementary to the other two, is given for predicting the distribution in the shallow fading range. All three methods are presented in step-by-step form for ease of application. The detailed bases of the methods, and their relationship to earlier methods, are also presented. These methods are the first to employ refractivity gradient statistics in the predictions and to cover the VHF/UHF bands in addition to the SHF band. Some guidance is also given to the designer on the path clearances required to minimize the effects of multipath fading.

De nouvelles méthodes sont présentées pour la prédiction de la distribution de l'affaiblissement du signal due à la propagation multivoie pour les mois moyen le plus difficile sur les liaisons terrestres en ligne de vue au Canada. Une première méthode pour les affaiblissements profonds ne requiert pas une information détaillée sur le profil à l'étude et elle est conçue pour les ébauches préliminaires et l'émission d'autorisations. Une seconde méthode nécessite la connaissance du profil détaillé du parcours et elle est destinée aux conceptions plus élaborées. Une troisième méthode, complémentaire aux deux premières, est adaptée à la prédiction de la distribution des affaiblissements moins profonds. Les trois méthodes sont présentées étape par étape pour que leur application soit plus facile. Les détails sur lesquels reposent ces méthodes et leurs relations avec les méthodes disponibles précédemment sont également présentés. Ces méthodes sont les premières à utiliser les statistiques sur le gradient de l'indice de réfraction dans les prédictions et à couvrir les bandes VHF/UHF en plus de le bande SHF. Quelques conseils sont aussi donnés sur le dégagement des parcours requis pour minimiser les effets de l'affaiblissement multivoie.

## Introduction

For over fifteen years, designers of terrestrial microwave line-of-sight links in Canada have almost universally used the techniques of Barnett [1] and Vigants [2] developed in the United States for predicting the deep fading range of the multipath fading distribution for individual hops. More recently, link designers in British Columbia [3] have used the technique of Morita [4] developed in Japan. The basis for this change is a fairly extensive set of measurements carried out in British Columbia [5], and comparisons with both the methods for the US and Japan which showed the Japanese method to be more accurate for this similarly mountainous province. Although the forms of the empirical equations are very similar, the "geoclimatic factor" model for Japan results in the prediction of significantly less severe fading in the average worst month than does that for the US.

In the planning and design of line-of-sight hops in the VHF/UHF bands, even less satisfactory prediction approaches have been applied. The best of these have been the Barnett-Vigants technique [2] for the upper UHF band and the curves of Bullington [6] for both the VHF and the UHF bands. The Barnett-Vigants technique, however, was based on data for the SHF band, and there has been no experimental or theoretical justification for its use at UHF. The Bullington curves were based on few observational data, with no allowance for geoclimatic variability. In the prediction of the shallow fade depth range of the clear-air fading distribution for the average worst month, there has been no technique available for any band that allowed for geoclimatic variability.

This paper presents two methods for predicting the deep fading range of the average worst-month multipath fading distribution on line-of-sight links in the upper VHF, UHF, and SHF bands in Canada. Method 1 does not require detailed path profile information and is best suited for preliminary planning or licensing purposes. In fact, an earlier, nearly identical version has already been adopted by the Department of Communications for licensing purposes in the VHF/UHF bands. It requires only path length, frequency and path inclination as input variables. Method 2, which is more appropriate for link design, also requires the "average" grazing angle of the wave specularly reflected from the ground, and therefore the path profile must be known. In addition to these two methods for the deep fading range, a compatible method is presented for the shallow fading range that also allows for geoclimatic variability. All three methods are first presented in step-by-step form for ease of application. The detailed bases of the methods, and their relationship to earlier methods, are then discussed following the step-by-step presentation. Some guidance is also given to the link designer on path clearances required to minimize the effects of multipath fading. It is suggested, for example, that a rigid application of standard path clearances rules may not be necessary or desirable in some cases.

The systematic analysis of a large British-French SHF data base that led to the development of the empirical prediction equations at

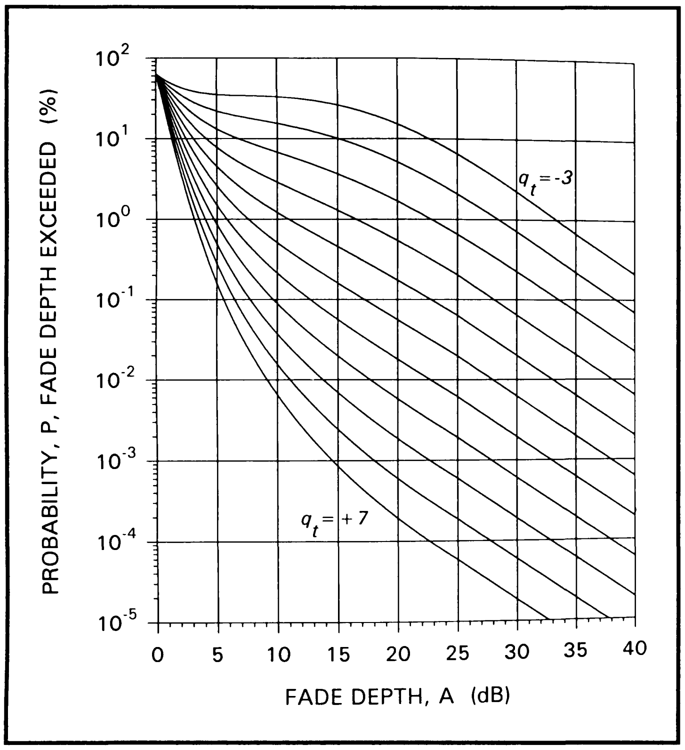


**Figure 1:** *Family of cumulative distributions of multipath fading typical for the average worst month (fade depth A exceeded for P per cent of the time) that results from an application of Methods 1 and 2 for the deep fading range ($A > 25$ dB if the shape factor $q_t > 0$, and $A > 35$ dB if $q_t < 0$), and the procedure for the shallow fading range (curves in increments of 1 for $q_t$).*

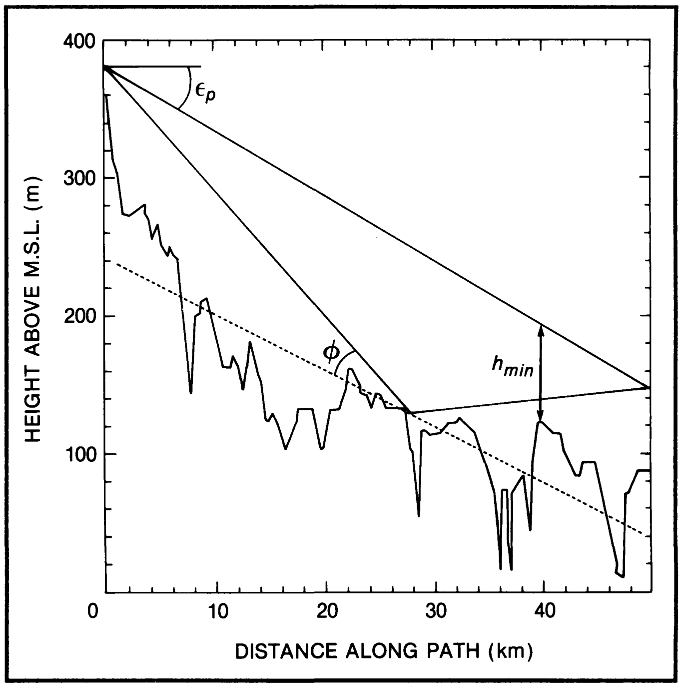


**Figure 2:** *Illustration of the link variables $\epsilon_p$ and $\phi$ for a typical path, with path profile shown on a flat-earth plot.*

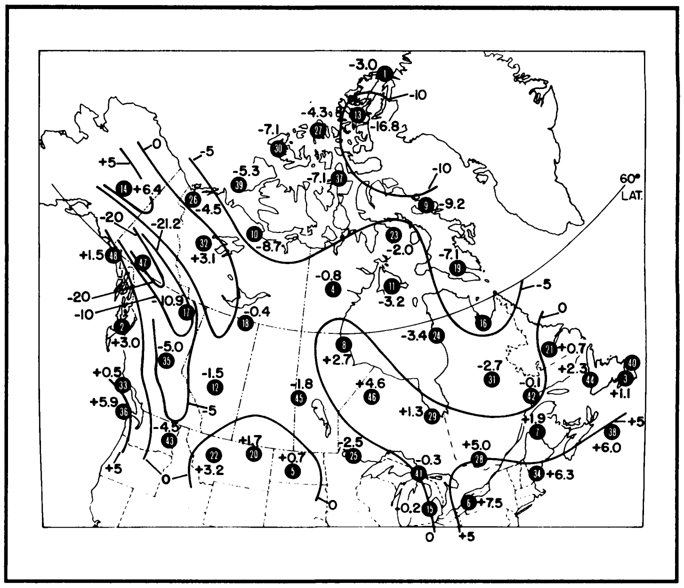


**Figure 3:** *Contour map indicating logarithmic geoclimatic factor G for Canada. The locations for which specific values of G are indicated are listed in Table III-1 of CRC Report 1315 [29].*

the heart of Methods 1 and 2 has been discussed by Tjelta et al. [7], and in somewhat less detail in three earlier publications [8]-[10]. Besides presenting Methods 1 and 2 in step-by-step form for Canadian link designers, the current paper concentrates on the means of extending the basic prediction equations (developed from the British-French data) to both the Canadian land mass using Canadian fading and meteorological data, and the VHF/UHF bands.

Earlier, almost identical, unpublished versions of Methods 1 and 2 developed for Canada and based on essentially the same British-French-Canadian data base have been recently extended for worldwide application and adopted by the International Radio Consultative Committee (CCIR) [11]. These worldwide CCIR versions employ refractivity gradient maps that, although giving worldwide coverage, do not have the high resolution available from the Canadian refractivity gradient data base and maps used here. Another paper [12] describes the means by which the initial versions of Methods 1 and 2 were extended worldwide, and presents the results of tests on the methods using data for several countries around the world. The detailed basis of the prediction method for shallow fade depths has been presented by Martin [13], and the results of comparisons of predictions with experimental data have been given elsewhere as well [12], [14].

## Step-by-step procedures

A family of cumulative distributions of multipath fading typical for the average worst month (fade depth $A$ exceeded for $P$ per cent of the time) that results from an application of the step-by-step procedures that follow is illustrated in Fig. 1. Methods 1 and 2, which are used for predicting the deep fading range of the distribution ($A > 25$ dB or $A > 35$ dB, depending on the value of the "shape factor," $q_t$), are presented first, followed by the method for the shallow fading range. Both Methods 1 and 2 use a "logarithmic geoclimatic factor," $G$, in the prediction process, which is a measure of the statistical occurrence of "ducts" near the surface in an average worst month for the link in question [7]. In addition, Method 1 uses the link variables of path length, $d$ (km); frequency, $f$ (GHz); and path inclination, $\epsilon_p$ (mrad). Besides $G$ and these three link variables, Method 2 also requires the grazing angle, $\phi$ (mrad), of the wave specularly reflected from the "average" path profile. The method for the shallow fading range employs the shape factor, $q_t$, which is a function of the other prediction variables. The link variables, $\epsilon_p$ and $\phi$, are illustrated in Fig. 2 for a typical path.

### Method for initial planning or licensing purposes (Method 1)

This method, which is for predicting the large fade depth range of the fading distribution for the average worst month, should normally be used for planning or licensing purposes or when the path profile is not known. The step-by-step procedure is as follows:

i) For the path location in question, obtain the logarithmic geoclimatic factor $G$ (in dB) for the average worst month, from the map in Fig. 3. This map shows contours of constant $G$, as well as

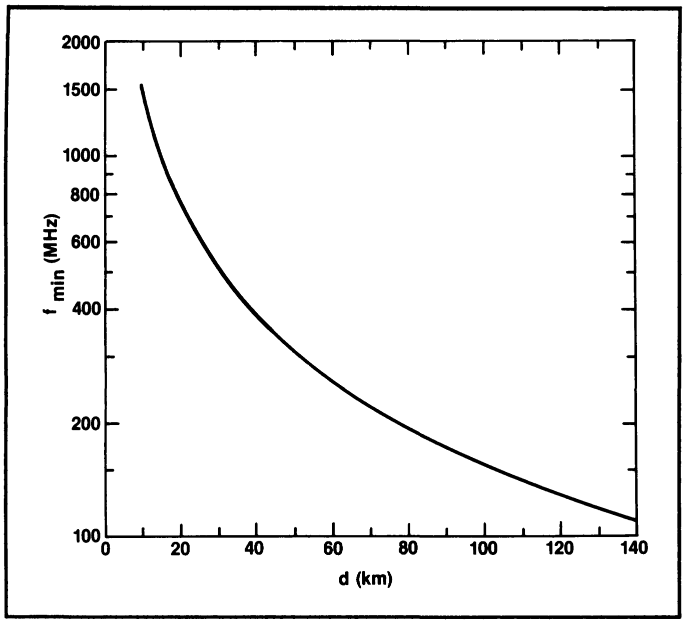


**Figure 4:** *Frequency below which the prediction methods are expected to be inaccurate, as a function of path length for $h_{min} \geq 77$ m.*

estimated values for 47 radiosonde sites across Canada and adjacent parts of the US. An approximate value for the path can be estimated by interpolation. If the path is above 60° latitude, add 5 dB to the value obtained from the map. If the path is over a medium-sized body of water (e.g. Bay of Fundy, Strait of Georgia, Frobisher Bay, Lake Ontario, Lake Erie), add 6 dB to the value of $G$ obtained from the map (i.e., 5 + 6 dB above 60° latitude). Finally, if the path is over a large body of water, particularly one for which there are no adjacent hills that might give rise to duct-inhibiting turbulence (e.g., Hudson Strait, Viscount Melville Sound, Hecate Strait, Cabot Strait, Lake Superior, Lake Huron, and perhaps Lake Michigan), add 14 dB to the value obtained from the map (5 + 14 dB above 60° latitude). In cases of uncertainty as to the size of the body of water in question, a 10 dB correction factor could be employed. (Particularly for over-water paths or paths above 60°, it may be useful to refer to the later section on limitations and accuracy of the models.)

ii) If the transmitting and receiving antenna heights, $h_e$ and $h_r$ (in metres above some reference height such as mean sea level), are known for the path of length $d$ (km), calculate the magnitude of the path inclination $|\epsilon_p|$ in milliradians from

$$|\epsilon_p| = 1000 \text{ Arctan}[\,|h_r - h_e|/1000d] \approx |h_r - h_e|/d. \quad (1)$$

If the antenna height difference has not yet been established, assume $|\epsilon_p| = 0$ or some other appropriate value.

iii) Calculate the percentage of time, $P$ (%), that fade depth $A$ (dB) is exceeded in the average worst month from the power-law expression

$$P = Kd^{3.6}f^{0.89}(1 + |\epsilon_p|)^{-1.4} \cdot 10^{-A/10}, \quad (2)$$

where $K$ is the geoclimatic factor given by

$$K = 10^{((G/10)-5.7)}. \quad (3)$$

Alternatively, calculate the fade depth $A$ (dB) exceeded for $P$ per cent of the time in the average worst month from

$$A = G - 57 + 36 \log d + 8.9 \log f$$
$$- 14 \log(1 + |\epsilon_p|) - 10 \log P. \quad (4)$$

Depending on the value of $G$ and the three link variables $d$, $f$, and $|\epsilon_p|$, (2) and (4) are valid for $A > 25$ dB or $A > 35$ dB. To determine which is the case, the interpolation procedure for shallow fade depths described below must be applied. A less stringent criterion [11], but one that need not be of concern if this procedure is applied, is that (2) and (4) are valid for $A > 15$ dB or the value exceeded for 0.1% of the worst month, whichever is greater.

Equations (2) and (4) were developed using data for path lengths in the range of 7.5 to 95 km, and frequencies in the range of 2 to 37 GHz. The results of measurements and analysis discussed later, however, suggest that they are valid at least down to the frequency indicated as a function of path length in Fig. 4 (see also (24), particularly for minimum path clearances $h_{min} < 77$ m). The same analysis provides a minimum path length for validity at a given frequency (here, (24) or Fig. 4 must be inverted). As indicated in a later discussion of one set of multifrequency results, (2) and (4) may be valid also for path lengths at least as large as 189 km. Path clearances contained in the data base covered a range of values [7] that resulted from the application of standard clearance rules for the SHF band in France and the UK [11]. As discussed later, (2) and (4) are likely to be conservative (fade depths overpredicted) for clearances either significantly less or significantly greater than normal. Some guidance on setting path clearance is given in the second last section.

**Method requiring path profile (Method 2)**

This method is best suited for link design applications. In addition to the path length, $d$ (km); frequency, $f$ (GHz); and path elevation angle, $\epsilon_p$ (mrad), it requires that the grazing angle, $\phi$ (mrad), of the wave specularly reflected from the "average" path profile be known. This necessitates the availability of the actual path profile. The step-by-step procedure is as follows:

i) Obtain the logarithmic geoclimatic factor $G$ as in Method 1, including the over-water and/or Arctic correction factors if required.

ii) Obtain the magnitude of the path inclination, $|\epsilon_p|$ (mrad), as in Method 1.

iii) From the profile of the terrain along the path, obtain the terrain heights, $h$, at intervals of 1 km, beginning 1 km from one terminal and ending 1 km to 2 km from the other. Using these heights, carry out a linear regression with the "method of least squares" to obtain the linear equation of the "average" profile:

$$h(x) = a_0 + a_1 x, \quad (5)$$

where $x$ is the distance along the path from the transmitter. The coefficients can be calculated from the relations [15],

$$a_0 = (\Sigma h - a_1 \Sigma x)/n, \quad (6)$$

$$a_1 = \frac{\Sigma xh - (\Sigma x \cdot \Sigma h)/n}{\Sigma x^2 - (\Sigma x)^2/n}, \quad (7)$$

where the summations are over the number, $n$, of profile height samples. From (5), calculate $h(0)$ and $h(d)$, the heights of the average profile at the ends of the path, and the heights of the antennas above the average path profile:

$$h_1 = h_e - h(0), \quad (8.1)$$

$$h_2 = h_r - h(d). \quad (8.2)$$

For paths where the point of specular reflection is fairly obvious (such as on paths over water, partially over water, or partially over flat, level terrain), the height above the reflecting surface should be used for $h_1$ and $h_2$. Also, on paths where a rigid application of the regression interval indicated above (i.e., to within 1 km of the ends of the path) would give obvious errors in the calculation of the "average" grazing angle (even though it is known to apply statistically [7]), it is suggested that a smaller regression interval over the path profile be chosen. On long paths, an increase in the profile sample distance to 2 km or more might be acceptable. After some experience with these more rigorous procedures involving linear regression, on some paths it may be possible to draw by eye a fairly accurate mean path profile in the vicinity of the reflection point.

If the path is so rough that it is obvious the main wave interaction with the ground would be one of diffraction from irregular mountain peaks rather than reflection from relatively flat surfaces, it may be meaningless to attempt to determine an appropriate value for the average grazing angle. For such a path, it is suggested that Method 1 be applied, and that the value of $G$ estimated from the map of Fig. 1 be reduced by 2 dB.

iv) Calculate the "average" grazing angle, $\phi$ (mrad), corresponding to a 4/3-earth radius model for refraction (i.e., $a_e = 8500$ km) from

$$\phi = \frac{h_1 + h_2}{d}\,[1 - m(1 + b^2)\,], \tag{9}$$

where

$$m = \frac{d^2}{4a_e(h_1 + h_2)}, \tag{10}$$

$$\varsigma = \frac{|h_1 - h_2|}{h_1 + h_2}, \tag{11}$$

$$b = 2\sqrt{\frac{m+1}{3m}}\,\cos\left[\pi/3 + \frac{1}{3}\,\mathrm{Arcos}\left(\frac{3\varsigma}{2}\sqrt{\frac{3m}{(m+1)^3}}\right)\right]. \tag{12}$$

Assume a minimum value for $\phi$ of 1 mrad. In calculation of the coefficients $m$ and $\varsigma$, the variables $a_e$, $d$, $h_1$ and $h_2$ must be in the same units. The grazing angle $\phi$ will be in the desired units of milliradians if $h_1$ and $h_2$ are in metres and $d$ in kilometres. If desired, the distances $d_e$ and $d_r$ from terminals $e$ and $r$ to the point of specular reflection on the average profile can be determined from

$$d_e = (1 \pm b)d/2 \begin{cases} h_1 > h_2 \\ h_1 < h_2 \end{cases} \tag{13.1}$$

and

$$d_r = (1 \mp b)d/2 \begin{cases} h_1 > h_2 \\ h_1 < h_2 \end{cases}. \tag{13.2}$$

Such calculations can be useful in choosing a suitable regression interval on the path profile.

v) Calculate the percentage of time, $P$, that the fade depth, $A$ (dB), is exceeded in the average worst month from

$$P = Kd^{3.3}f^{0.93}(1 + |\epsilon_p|)^{-1.1}\phi^{-1.2}\cdot 10^{-A/10}, \tag{14}$$

where $K$ is the geoclimatic factor given by

$$K = 10^{((G/10)-4.6)}. \tag{15}$$

Alternatively, calculate the fade depth, $A$ (dB), exceeded for $P$ per cent of the time from

$$a = G - 46 + 33\log d + 9.3\log f - 11\log(1 + |\epsilon_p|) - 12\log\phi - 10\log P. \tag{16}$$

The minimum ranges of variables over which (14) and (16) should apply are the same as those indicated with (2) and (4), with the addition of the range $\phi < 14$ mrad [7].

**Interpolation procedure for shallow fade depths**

This empirical procedure has been designed to predict that portion of the fading distribution for the average worst month between 0 dB and the deep fading levels predicted by Methods 1 and 2. In step-by-step form, it is as follows:

i) Using Method 1 or 2 as appropriate, calculate the percentage of time, $P$(35 dB), that a fade depth of 35 dB is exceeded in the "tail" of the distribution (i.e., (2) or (14)).

ii) Calculate the value of the parameter $q'$ corresponding to the fade depth $A = 35$ dB and $P = P(35\text{ dB})$ from

$$q' = -\frac{20}{A}\log_{10}\left[-\ln\left(\frac{100 - P}{100}\right)\right]. \tag{17}$$

iii) Calculate the value of the shape factor $q_t$ from

$$q_t = (q' - 2)/[(1 + 0.3\cdot 10^{-A/20})\cdot 10^{-0.016A}] - 4.3(10^{-A/20} + A/800). \tag{18}$$

iv) If $q_t > 0$, repeat steps i) to iii) for $A = 25$ dB.

v) For $0 < A < 25$ dB or $0 < A < 35$ dB, as appropriate, calculate the percentage of time, $P$, that $A$ is exceeded from

$$P = 100[1 - \exp(-10^{-qA/20})\,], \tag{19}$$

where $q$ is also a function of $A$ given by

$$q = 2 + 10^{-0.016A}[1 + 0.3\cdot 10^{-A/20}] \times [q_t + 4.3(10^{-A/20} + A/800)\,]. \tag{20}$$

Alternatively, calculate the fade depth, $A$ (dB), exceeded for $P$ per cent of the time from

$$A = -\frac{20}{q}\log_{10}\left[-\ln\left(\frac{100 - P}{100}\right)\right]. \tag{21}$$

The method is valid for values of $q_t$ greater than about $-3$, which covers virtually all the combined ranges of $G$, $d$, $f$, $|\epsilon_p|$, and $\phi$ values likely to arise under operational circumstances in Canada. For values of $q_t$ less than about $-3$, the shape of the model distribution becomes nonphysical.

## Background to the methods

**The basic microwave tail models**

Equations (2) and (14) (or (4) and (16)) are three- and four-variable models (four and five variables with the geoclimatic factor) based on microwave data for the large fade depth tail portion of the fading distribution for the average worst month. The tail portion of the distribution as expressed by these equations has the Rayleigh slope of 10 dB/decade and occurs for fade depths greater than about 15 dB on average. It is believed to be caused by a combination of atmospheric fading (largely beam spreading of the direct wave, commonly referred to as defocussing) and surface reflection [16]-[17].

With the possible exception of minor variations discussed by Tjelta et al. [7], these three- and four-variable models [10] are believed to be the most accurate "tail" models currently available [12], [18]. They were developed as part of an effort by Interim Working Party 5/2 (now WP 5C) of CCIR Study Group 5 [19] to improve prediction methods for microwave frequencies [9]. They

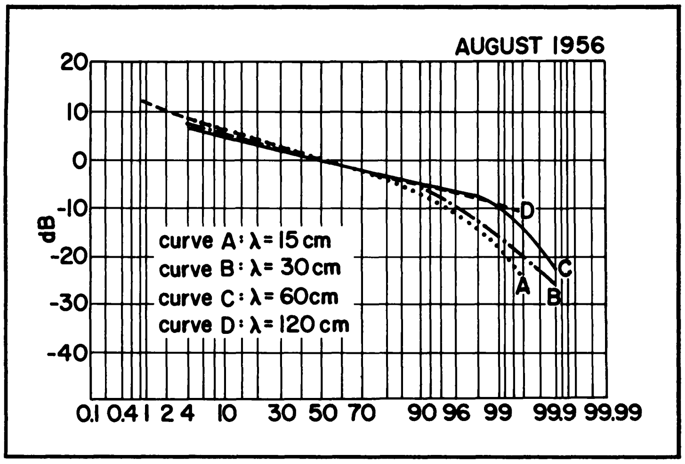


**Figure 5:** *Worst-month fading distributions in 1956 for 189 km path, Mount Cimone-Milan, Italy, at 250 MHz, 500 MHz, 1 GHz and 2 GHz (after Carassa and Quarta [24]).*

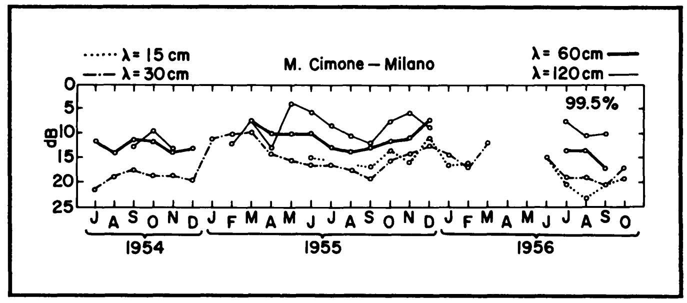


**Figure 6:** *Monthly fade depths exceeded for 99.5% of the time for the three-year period 1954-1956 on the path indicated (after Carassa and Quarta [24]).*

were based on a fading data base for 47 links in France and the UK, considerably larger than the number used in the Barnett-Vigants model [1]-[2] for the US, the Doble model [11], [20] for the UK, or the old regional model for North-Western Europe [21] still cited by the CCIR [11].

The new models also incorporate improved analytical procedures [7]. The earlier models were based on fits at either constant probability or constant fade depth levels of the distribution. Errors were caused by the fact that for some links, these levels were not in the tail of the fading distribution. In developing the new "tail" models, the fade depths were chosen specifically so that they would be in the distribution tails and have the highest exceedance probabilities possible within this constraint, in order to maximize statistical stability. These minimum tail fade depths were then scaled to a fixed probability level using the average 10 dB/decade Rayleigh slope, before the model fitting was carried out.

Another improvement in the modelling is that worst-month fading distributions are treated with greater statistical consistency. In some previous analyses, for example, the worst one-month distributions over different measurement durations were mixed (i.e., worst-month distributions for one year were combined with those for two years, three years, etc., in the fitting). Such mixed statistics have a bias with respect to each other (i.e., four-year worst-month fade depths tend to be larger than three-year fade depths, etc.), and those associated with the longest overall durations of measurement have very large standard errors. The approach employed in the new analysis [7], [9]-[10] was to use the average worst-month distribution envelope [22], whatever the number of years. Clearly, with this approach the standard error of one-year worst-month statistics is greater than that of two-year averages, etc., but there is no bias. The fit is therefore more accurate.

The major improvements in the new models have resulted from the use of multiple regression and multiple iteration [7], [9]-[10] in fitting the power-law equations to the fading data. Multiple regression gives the most accurate relationship between the exponents in the power law, and multiple iteration allows the geoclimatic factor to vary from one region to another, at the same time increasing the accuracy of the multiple regression.

Various other statistical tests and correlation analyses of errors were used to determine the most significant prediction variables [7], [10]. One major finding of these analyses is that the path inclination is a more significant variable than the surface roughness variable originally introduced by Pearson [23] and later employed by Vigants [2]. The relevance of surface roughness in the Barnett-Vigants model [2] is explained by two factors: a) a large component of the surface roughness is often the average terrain inclination, which is highly correlated with the path inclination; and b) there is a tendency for the roughest paths to have the largest path inclinations. Another important outcome of the analysis is that the "average" grazing angle, $\phi$, of the ground-reflected wave is a significant prediction variable. The physical bases of all the prediction variables have been considered in some detail elsewhere [7], [16].

**Extrapolation of the microwave tail models to VHF/UHF**

There are not enough VHF and UHF data available anywhere in the world to allow the direct development of empirical models for these bands giving close to the same degree of confidence as those for the SHF band. After some investigation, it was felt that the best prediction approach for the VHF and UHF bands would be to extrapolate downwards in frequency from the basic microwave tail models discussed earlier. There are enough data available for testing, and the physical mechanisms that cause fading at both SHF and VHF/UHF are sufficiently well understood [16]-[17], to lend confidence to this approach.

The most useful data are those that have been obtained at multiple frequencies within the VHF/UHF/SHF bands. The frequency term in the prediction equations can then be evaluated without the need to know the geoclimatic factor. A particularly good set of measurements at four frequencies (250 MHz, 500 MHz, 1 GHz, 2 GHz) was obtained over a six-year period on a 189 km path in Italy [24]-[25]. The fading distributions for the worst month in this six-year period are reproduced in Fig. 5, and the month-by-month 99.5% (tail) levels for a three-year period, in Fig. 6. As is evident from Fig. 5, the distributions for the three higher frequencies have tails beginning at about 10 dB. (The dynamic range of the receiver at the lowest frequency was insufficient for the tail to be observed.) More importantly, both Figs. 5 and 6 suggest that for the summer months, there is an average difference of approximately 2.8 dB between the distribution tails at adjacent frequencies for a given percentage of time. This is the approximate difference predicted by Method 2. As a second check, the appropriate geoclimatic factor was calculated from the 2 GHz data for August 1956, by working backwards from the three-variable model of (2); the result was found to be identical to the average value for the adjacent Dijon area of France [7]. (This check also suggests that Methods 1 and 2 are at least approximately valid for path lengths at least as large as 189 km.)

Another important set of multifrequency measurements (45.1 MHz, 474 MHz and 2.81 GHz) was obtained for a 68 km path on New York's Long Island [26]. At 0.1% of the worst month, which is in the distribution tails at both 47[illegible] nd 2.8 GHz, the measured difference in fade depth at these [illegible] ies is 8.5 dB as compared to a predicted value of 7.2 dB wit[illegible] 1 2. Such agreement is very good. The 45.1 MHz distributior [illegible] t exhibit a tail for the fade depths measured, and the median level suggests that there is considerable destructive interference between the direct and ground-reflected waves even under normal conditions. A calculation from the 2.8 GHz distribution using the three-variable model (4) gives $G = 10.6$ dB, and a calculation using the four-variable model (6) gives [illegible] for this region of the US (see Fig [illegible]

**Table 1**
**Data and characteristics of experimental links in Canada**

| Link [Reference] (Path coordinates) | Ant. Ht. (m) Above Ground Tx | Rx | $d$ (km) | $f$ (GHz) | $\lvert\epsilon_p\rvert$ (mrad) | $\phi$ (mrad) | Measurement period (Worst month) | Tail $A$ (dB) | Tail $P$ (%) | Observ. $G$ (dB) (Eqn. 4) | Observ. $G$ (dB) (Eqn. 16) | Predict. $G$ (dB) (Fig. 3) | Remarks |
|---|---|---|---|---|---|---|---|---|---|---|---|---|---|
| 1. Corkery-Shirley Bay, Ont. [32]<br>(45°16′16″N, 77°3′44″W-45°20′52″N, 76°52′58″W) | 18 | 40 | 16.3 | 10.8 | 3.55 | 3.8 | May-Sep 1979 | 25.8 | 0.001 | 9.8 | 7.3 | 5.0 | Reference link. |
| 2. Corkery-Shirley Bay, Ont. [32] | 18 | 40 | 16.3 | 11.08 | 3.55 | 3.8 | May-Sep 1979 | 29.3 | 0.001 | 13.1 | 10.7 | 5.0 | Reference link. |
| 3. Corkery-Shirley Bay, Ont. [32] | 18 | 40 | 16.3 | 16.53 | 3.55 | 3.8 | May-Sep 1979 | 18.0 | 0.001 | 0.3 | −2.2 | 5.0 | Reference link. |
| 4. Corkery-Shirley Bay, Ont. [32] | 18 | 40 | 16.3 | 16.81 | 3.55 | 3.8 | May-Sep 1979 | 19.9 | 0.001 | 2.2 | −0.4 | 5.0 | Reference link. |
| 5. Kingsmere-Shirley Bay, Ont. [32]<br>(45°29′17″N, 75°51′21″W-45°20′52″N, 76°52′58″W) | 18 | 40 | 15.7 | 11.35 | 15.5 | 22.2 | May-Sep 1979 | 12.0 | 0.001 | 4.2 | 9.6 | 5.0 | Surface reflection on Ottawa River. Reference link. |
| 6. Kingsmere-Shirley Bay, Ont. [32] | 18 | 40 | 15.7 | 17.71 | 15.5 | 22.2 | May-Sep 1979 | 15.3 | 0.001 | 5.8 | 11.1 | 5.0 | Surface reflection on Ottawa River. Reference link. |
| 7. Kemptville-Avonmore, Ont. [36]<br>(44°59′57″N, 75°33′18″W-45°08′47″N, 74°56′48″W) | 63 | 78 | 50.5 | 3.65 | 0.326 | 2.1 | 11 Jun-29 Jul 1985 | 16.2 | 0.311 | 4.1 | 1.8 | 5.0 | Reference link. |
| 8. Kemptville-Avonmore, Ont. [36] | 63 | 65 | 50.5 | 3.65 | 0.079 | 1.9 | 11 Jun-29 Jul 1985 | 16.4 | 0.424 | 4.5 | 1.7 | 5.0 | Reference link. |
| 9. Kemptville-Avonmore, Ont. [31] | 63 | 78 | 50.5 | 8.05 | 0.326 | 2.1 | 9 Aug-12 Sep 1977 | 16.0 | 1.95 | 8.9 | 6.4 | 5.0 | Reference link. |
| 10. Kemptville-Avonmore, Ont. [31] | 63 | 65 | 50.5 | 8.05 | 0.079 | 1.9 | 9 Aug-12 Sep 1977 | 16.0 | 1.35 | 6.7 | 3.9 | 5.0 | Reference link. |
| 11. Kemptville-Avonmore, Ont. [31] | 63 | 25 | 50.5 | 8.05 | 0.730 | 1.0 | 9 Aug-12 Sep 1977 | 22.0 | 0.14 | 5.1 | −1.4 | 5.0 | 0.6 Fresnel zone clearance. $G$ value not included in average for Ottawa. |
| 12. Firth-Tabor, B.C. [5]<br>(54°48′45″N, 122°46′11″W-53°54′44″N, 122°27′01″W) | 6 | 6 | 102.3 | 7.5 | 1.98 | 3.9 | Jul 1981-Oct 1982 (Sep 1982) | 15.0 | 0.197 | −7.8 | −7.0 | −5.0 | Reference link. |
| 13. McEwan-Tabor, B.C. [5]<br>(54°24′11″N, 122°29′45″W-53°54′44″N, 122°27′01″W) | 11 | 9 | 54.7 | 3.8 | 2.5 | 18.7 | Jul 1981-Oct 1982 (Sep 1982) | 15.0 | 0.0077 | −8.6 | −0.5 | −5.0 | Reference link. |
| 14. Hixon-Tabor, B.C. [5]<br>(53°28′43″N, 122°38′00″W-53°54′44″N, 122°27′01″W) | 53 | 57 | 49.8 | 3.9 | 9.3 | 5.5 | Jul 1981-Oct 1982 (Sep 1982) | 20.0 | 0.0011 | −4.0 | −3.7 | −5.0 | Reference link. |
| 15. Cluculz-Frazer, B.C. [5]<br>(53°54′54″N, 123°27′25″W-54°01′51″N, 124°37′21″W) | 15 | 27 | 77.8 | 7.2 | 2.63 | 6.0 | Apr 1980-May 1981 (July 1980) | 20.0 | 0.0119 | −9.3 | −6.4 | −5.0 | Reference link. |
| 16. Cluculz-Frazer, B.C. [5] | 15 | 27 | 77.8 | 7.5 | 2.63 | 6.0 | Apr 1980-May 1981 (Sep 1980) | 20.0 | 0.0085 | −11.0 | −8.1 | −5.0 | Reference link. |

Another early set of multifrequency measurements (9.4 GHz, 4.6 GHz, 3 GHz and 714 MHz) was obtained by Durkee [27] over a 64 km path, also in New York state. Although the 714 MHz data were not obtained over exactly the same period as the higher frequency data, the differences in the distributions are reasonably consistent with the model. The differences between distributions measured during two different time periods at 300 MHz and 3 GHz on a 160 km path in Switzerland [28] are also reasonably consistent with the model.

An important consideration in applying the Rayleigh tail models ( (2) and (14) ) is the minimum frequency for which they are valid. As discussed elsewhere [16], the tail is believed to result primarily from the combination of atmospheric fading due to ducts in proximity to the path, and surface reflections. The most likely situation to cause atmospheric fading such that the atmospheric signal and the surface-reflected signals can interfere sufficiently destructively with one another occurs when the centre of the duct is located just below the path [16]. Here the atmospheric fading and the phase shift between the direct and surface-reflected waves are simultaneously greatest for a duct of given intensity.

This "relative maximum" phase shift can be estimated [16] from

$$\Delta\phi_m = 2\pi f(\Delta\tau_1 + \Delta\tau_2) + \pi, \tag{22}$$

where $\Delta\tau_1$ is the geometric delay difference within a normal atmosphere, $\Delta\tau_2$ is the additional contribution due to the presence of a duct just below the path, and $\pi$ is the phase shift introduced in surface reflection. The duct contribution, $\Delta\tau_2$, is normally much larger than $\Delta\tau_1$ and can be estimated [16] from

$$\Delta\tau_2 \approx 0.8(\lvert\Delta N\rvert \cdot 10^{-6})d/c, \tag{23}$$

where $\lvert\Delta N\rvert$ is the intensity of the duct (i.e., the difference in refractivity between the bottom and the top of the duct) in $N$ units, $d$ is the path length, and $c$ is the speed of light.

Ignoring the usually small value of $\Delta\tau_1$ and assuming a duct intensity of 12.1 $N$ units over a path whose minimum clearance, $h_{min}$, under ducting conditions (obtained from a flat-earth plot such as that in Fig. 2, with exclusion intervals of at least 1 km at the ends of the path to avoid hills on which the antennas are situated) is greater than 77 m (i.e., intensity due to a duct threshold gradient of $-157$ $N$ units/km over a duct thickness of 77.3 m, the average surface duct thickness in Canada [29]), we obtain $\Delta\phi_m \approx 2\pi(9.7 \cdot 10^{-6})fd/c + \pi$. Furthermore, for a path with $h_{min} < 77$ m, we obtain $\Delta\phi_m \approx 2\pi(9.7 \cdot 10^{-6})fdh_{min}/77c + \pi$. If the minimum value of $\Delta\phi_m = 2\pi$ is taken, allowing for a relatively uniform distribution of the phase between direct and surface-reflected waves, this gives a quasi-minimum frequency of

$$f_{min} = \begin{cases} \dfrac{1.6 \cdot 10^4}{d} \text{ (MHz)} & \text{for } h_{min} \geq 77 \text{ m} \\ \dfrac{1.2 \cdot 10^6}{dh_{min}} \text{ (MHz)} & \text{for } h_{min} < 77 \text{ m} \end{cases}, \tag{24}$$

**Table 1** *(cont'd)*
**Data and characteristics of experimental links in Canada**

| Link [Reference] (Path coordinates) | Ant. Ht. (m) Above Ground Tx | Rx | $d$ (km) | $f$ (GHz) | $\lvert\epsilon_p\rvert$ (mrad) | $\phi$ (mrad) | Measurement period (Worst month) | Tail $A$ (dB) | Tail $P$ (%) | Observ. $G$ (dB) (Eqn. 4) | Observ. $G$ (dB) (Eqn. 16) | Predict. $G$ (dB) (Fig. 3) | Remarks |
|---|---|---|---|---|---|---|---|---|---|---|---|---|---|
| 17. Creston-Salmo, B.C. [5]<br>(49°05′35″N, 116°22′45″W-49°04′18″N, 117°04′56″W) | 17 | 15 | 51.4 | 4.1 | 0.89 | – | Feb-Oct 1982<br>(Feb 1982) | 25.0 | 0.0006 | −11.2 | – | −4.5* | Rough, mountainous terrain. |
| 18. Rossland-Salmo, B.C. [5]<br>(49°05′35″N, 117°47′50″W-49°04′18″N, 117°04′56″W) | 6 | 13 | 52.3 | 6.9 | 17.1 | – | Feb-Oct 1982<br>(Oct 1982) | 15.0 | 0.0022 | −5.5 | – | −5.0* | Rough, mountainous terrain. |
| 19. Santa Rosa-Salmo, B.C. [5]<br>(49°01′27″N, 118°03′31″W-49°04′18″N, 117°04′56″W) | 11 | 15 | 71.6 | 4.1 | 6.5 | – | Feb-Oct 1982<br>(Oct 1982) | 20.0 | 0.0105 | −2.0 | – | −5.0* | Rough, mountainous terrain. |
| 20. Blackwall-Hope, B.C. [5]<br>(49°06′05″N, 120°45′25″W-49°24′35″N, 121°33′28″W) | 18 | 11 | 67.6 | 3.8 | 8.2 | – | Feb 1981-May 1982<br>(Dec 1981) | 15.0 | 0.0038 | −9.0 | – | −2.0* | Rough, mountainous terrain. |
| 21. Hope-Chilliwack, B.C. [5]<br>(49°24′35′N, 121°33′28″W-49°06′52″N, 121°54′07″W) | 26 | 46 | 41.4 | 7.8 | 29.2 | 40.0 | Feb 1981-Oct 1982<br>(Jul 1982) | 15.0 | 0.0012 | −1.9 | 7.2 | 2.0 | |
| 22. Uniondale-London, Ont. [37]<br>(43°13′42″N, 81°02′18″W-43°00′25″N, 81°16′28″W) | 46 | 25 | 30.7 | 16.65 | 3.16 | 1.9 | 11 Jul-1 Nov 1986 | 7.5 | 5.0 | 16.4 | 11.2 | 5.0 | $P$ value reduced by 6% to account for rain attenuation [40]. |
| 23. Otter Lake, N.B.-Nictaux S, N.S. [38]<br>(45°22′10″N, 65°46′23″W-44°52′00″N, 65°02′10″W) | 69 | 81 | 80.4 | 9.5 | 0.684 | 5.7 | 31 Jul-3 Sep 1981 | 27.5 | 0.315 | 6.1 | 9.1 | 11.0<br>(5.0) | Oversea path with partial blockage of sea reflection. |
| 24. Big Sicker-Vancouver, B.C. [5]<br>(48°51′38″N, 123°45′20″W-49°16′52″N, 121°33′28″W) | 15 | 72 | 66.1 | 4.2 | 9.6 | 6.7 | Jul-Oct 1979<br>(Oct 1979) | 20.0 | 0.0961 | 10.9 | 12.5 | 10.0<br>(4.0) | 60% oversea path. |
| 25. Vancouver-Big Sicker, B.C. [5] | 70 | 15 | 66.1 | 8.2 | 9.6 | 6.7 | Jul-Oct 1980<br>(Jul 1980) | 20.0 | 0.0352 | 4.0 | 5.5 | 10.0<br>(4.0) | 60% oversea path. |
| 26. Lowther Peak-Martyr Peak, N.W.T. [39]<br>(74°31.8′N, 97°27.2′W-74°41.2′N, 95°2.9′W) | 7 | 7 | 72.0 | 0.468 | 0.125 | 3.0 | 2 Sep 1983-22 Apr 1984<br>4 Jun 1984-7 Jan 1985<br>(Oct 1983) | 22.8 | 0.1 | 7.2 | 2.4 | 11.9<br>(−7.1) | Arctic oversea path. |
| 27. Schomberg Peak-Cockburn Peak, N.W.T. [39]<br>(75°33.7′N, 105°35.1′W-75°1.8′N, 100°15.1′W) | 7 | 7 | 91.0 | 0.463 | 0.231 | 1.1 | 4 Jun 1984-7 Jan 1985<br>(Jul 1984) | 36.9 | 1.0 | 28.3 | 24.1 | 11.9<br>(−7.1) | Arctic oversea path with <0.6 Fresnel zone clearance. |
| 28. Cockburn Peak-Lowther Peak, N.W.T. [39]<br>(75°1.8′N, 100°15.1′W-74°31.8′N, 97°27.2′W) | 7 | 7 | 98.8 | 0.453 | 0.253 | 0.7† | 2 Sep 1983-10 Nov 1983<br>4 Jun 1984-7 Jan 1975<br>(Jul 1984) | 41.5 | 0.1 | 21.8 | 14.7 | 11.9<br>(−7.1) | Arctic oversea path with <0.6 Fresnel zone clearance. |
| 29. Cockburn Lake-Lowther Peak, N.W.T. [39]<br>(75°1.6′N, 100°10.0′W-74°31.8′N, 97°27.2′W) | 7 | 5 | 96.5 | 0.458 | 1.05 | 0.0† | 2 Sep 1983-20 Oct 1983<br>3 Aug 1984-7 Jan 1985<br>(Sep 1983) | 42.5 | 0.01 | 16.1 | 10.7 | 11.9<br>(−7.1) | Grazing oversea path in Arctic. |
| 30. Cape Warwick-Lacy, N.W.T. [30]<br>(61°36′N, 64°38′W-60°41′N, 64°35′W) | 6 | 6 | 101.7 | 0.465 | 1.24 | 2.87 | Dec 1986-Nov 1987<br>(Jun 1987) | 23.0 | 1.0 | 16.4 | 16.4 | 12.1<br>(−6.9) | Acrtic oversea path. |
| 31. Cape Warwick-Cape Cracroft, N.W.T. [30]<br>(61°36′N, 64°38′W-62°44′N, 65°18′W) | 6 | 6 | 131.9 | 0.453 | 0.48 | 2.11 | Dec 1986-Nov 1987<br>(Jul 1987) | 14.4 | 3.0 | 6.1 | 5.3 | 12.0<br>(−7.0) | Arctic oversea path. |
| 32. Cape Cracroft-Vanderbilt, N.W.T. [30]<br>(62°44′N, 65°18′W-63°04′N, 67°39′W) | 6 | 6 | 125.7 | 0.466 | 0.72 | 3.81 | Dec 1986-Nov 1987<br>(Sep 1987) | 12.6 | 2.0 | 4.1 | 6.2 | 3.9<br>(−7.1) | Arctic oversea path. |
| 33. Cape Vanderbilt-Iqaluit, N.W.T. [30]<br>(63°04′N, 67°39′W-63°45′N, 68°32′W) | 6 | 6 | 89.6 | 0.450 | 5.45 | 2.00 | Dec 1986-Nov 1987<br>(Sep 1987) | 10.5 | 0.1 | 2.4 | −0.9 | 3.9<br>(−7.1) | Actic oversea path. |

Notes: The predicted $G$ values in parentheses are values from Fig. 3 uncorrected for over-water and Arctic paths.
* The predicted $G$ values for the mountainous paths indicated by an asterisk must be reduced by 2 dB for Method 2, as discussed in the step-by-step procedure.
† In the two paths noted, $\phi$ = 1mrad assumed in observed $G$ calculations for 4-variable model (16), as discussed in the procedure for Method 2.

for threshold duct conditions, with $d$ in kilometres and $h_{min}$ in metres. A plot of $f_{min}$ as a function of path length is given in Fig. 4 for $h_{min} \geq 77$ m. It must be emphasized that $f_{min}$ will be smaller for larger duct intensities, and therefore distribution tails (i.e., with Rayleigh slope) will exist at lower frequencies. The limit expressed by (24) and Fig. 4 is meant only to give some indication of the frequency below which the accuracy of the Rayleigh tail model must be seriously questioned on physical grounds. (For the purposes of determining a minimum path length, $d_{min}$ (km), for approximate validity of the Rayleigh tail model at a given frequency $f$ (MHz), the independent and dependent variables in (24) or Fig. 4 can be inverted.)

**Interpolation procedure for shallow fade depths**

The basis of the method for low fade depths is described in more detail elsewhere [12]-[14]. It is essentially an empirical interpolation procedure which generates a smooth transition between the large fade depth Rayleigh tail range of the distribution described by Methods 1 and 2, and the fade depth of 0 dB. Tests on the method using extensive microwave data available for France and the UK show it to have mean residual errors of less than 1 dB and standard deviations of error of less than 3.2 dB in the exceedance probability range of 0.01% to 1% of the average worst month [12], [14]. There is no reason to believe that it would not perform as well in Canada. Once sufficient data for VHF/UHF links in Canada become available, including overland links, the accuracy of the method should be verified for this part of the spectrum. Since it is an interpolation procedure tied to the two tail methods, however, it is reasonable to expect, as observed for the British-French data [7], [14], that the errors for the tail methods are upper bounds on average to the errors of the interpolated curves.

## Radio-meteorological considerations

### Basis for geoclimatic factor variation

The propagation of radio waves through the troposphere is influenced by gradients in the refractive index. These gradients determine the curvature of the signal "rays" as they travel, and extreme values of gradients are responsible for anomalous propagation during clear-air conditions. The refractivity, $N$, defined as the difference between the actual refractive index at a point in the atmosphere and the refractive index *in vacuo* multiplied by $10^6$, is determined by the values of temperature, pressure and absolute humidity. A vertical refractivity gradient of approximately $-39$ $N$ units/km over the lowest 100 m is average for Canada [29]. Larger lapse rates (i.e., gradients $< -39$ $N$ units/km) are referred to as being "superrefractive." Gradients less than $-157$ $N$ units/km are designated as "ducting" gradients, while the overall height limits between which this condition prevails constitute the actual "duct."

Although the vertical structure of refractivity is known to be crucial to the tropospheric propagation of microwave signals far beyond the line of sight, its importance in terms of multipath on line-of-sight links is not yet as well appreciated. Two important considerations weight heavily on this problem. First of all, while low-lying superrefractive or ducting layers (i.e., below the level of the antennas) may give rise to abnormal spreading, or "defocussing," of the energy in the direct wave between the two antennas, and at the same time to an enhanced surface-reflected wave that interferes destructively with the direct wave [16]-[17], there is no precise point at which these conditions occur. Depending on the geometry of the situation, a duct may not be necessary at all for multipath propagation to occur. In other instances a rather large or very intense duct might be required.

The second consideration arises out of the practical limitations of most of the tropospheric refractivity statistics available. These statistics are generally derived from analysis of meteorological observations obtained using radiosondes, typically those launched by weather balloons for synoptic weather information. At the very low altitudes of concern to VHF-SHF radio links, these data are seriously lacking in both resolution and sensitivity. The net result is that many low-lying refractive structures are not recorded by the radiosonde system. In addition, the severity of rapidly varying layers is underestimated. Where a realistic estimate of the probability of duct occurrence is needed, it is actually likely to be more accurately approximated by the recorded incidence of superrefractive layers than by the noted occurrence of ducting gradients themselves. Coupled with these problems of spatial resolution and sensitivity are the additional limitations arising from the fact that the routine radiosonde measurements are taken only every 12 hours, with different local measurement times in each time zone.

### Choice of a suitable climatic variable to characterize fading

In view of the uncertainty regarding both the identity of the fundamental radio-meteorological variable of consequence and the lack of reliability in existing data, several possible predictor variables were examined. The results were then considered for meteorological significance and for consistency with available propagation data. The three-year data base used for this purpose was the same as that employed in a tabulation of duct occurrences contained in an earlier report [29], and includes all sites listed in Table III-1 of that report except St. John's, Nfld. These locations cover all of Canada, albeit thinly, and adjacent parts of the US.

The occurrences of both ducts and surface-based superrefractive layers were calculated. The data for surface ducts and elevated-surface ducts were merged, as it was felt that these conditions are likely to produce very similar progagation effects. Furthermore, since it was felt that data for a single worst month might be unreliable (because of normal fluctuations over a few years and the fact that one month might provide too small a sample), data were also examined for the worst two and the worst three calendar months. These were not necessarily successive months, nor the same months for ducts and superrefractive layer occurrences.

The superrefractive layer occurrences were found to provide a smooth pattern of variation across the country with very similar results for one-, two-, or three-calendar-month data. The duct probabilities also yielded geographically similar maps for one-, two-, or three-month averages. Perhaps because of the reduced number of occurrences, however, the duct probability maps displayed a less gradual or consistent pattern of variation over the entire land mass, particularly in the high Arctic.

From a climatological point of view, the superrefractive layer occurrence provided a more convenient variable for classifying anomalous refractivity conditions in Canada. On the other hand, when a regression relation was sought (see following section) between the different refractive parameters and the known fading characteristics at selected locations, it was found that the superrefractive layer occurrence predicted more extreme fading for southwestern Ontario and the northeastern corner of the US than seemed reasonable on the basis of the small sample of fading data available. The worst three-calendar-month average probability of occurrence of surface plus elevated-surface ducts was therefore used in the present model.

### Relationship between the geoclimatic factor and duct occurrence probability

Fortunately, enough fading data exist for various paths around the country so that prediction equations can be obtained in terms of the combined occurrence probability of surface and elevated-surface ducts. Table 1 presents these data and the associated path parameters. The fade depths, $A$, and time percentages, $P$, given correspond to the first points (i.e., highest percentage of time and lowest fade depth) that can reasonably be considered to be in the distribution tail (i.e., the deep fading portion with a slope of approximately 10 dB/decade) [7]. In most cases, either the complete distribution or enough points in it were available to permit these tail points to be determined relatively easily.

As far as possible, these data are for the worst calendar month of the overall measurement period, both of which are indicated in Table 1. The four paths for which this is not strictly true are Corkery-Shirley Bay, Kingsmere-Shirley Bay, Kemptville-Avonmore, and Otter Lake-Nictaux South. The first two are so short and the tail-point percentage so low (0.001%) that five-month averages were used. Furthermore, the fading for the Corkery-Shirley Bay path was fairly uniform throughout this five-month period. The data for the Kemptville-Avonmore and Otter Lake-Nictaux South paths should be effectively worst-month data because of the time intervals in which they were obtained.

The procedure followed in establishing a relationship between the logarithmic geoclimatic factor $G$ and duct occurrence, was to work backwards from the fading data to calculate $G$ for each link. This was done using both the three-variable equation (4) and the four-variable equation (16). Table 1 lists both sets of values, except for four paths in British Columbia where only the three-variable calculations are given. These paths are so rough that an accurate value for the "average" grazing angle, $\phi$, could not be established. Table 1 also lists the values of $G$ for the over-water and Arctic paths before and after the corrections indicated previously were applied. These are discussed in the next section.

The three paths in the Ottawa area (Corkery-Shirley Bay, Kingsmere-Shirley Bay, Kemptville-Avonmore) and the four paths in the Prince George area (Firth-Tabor, McEwan-Tabor, Hixon-Tabor, Cluculz-Fraser) currently provide the best basis on which to establish the relationship between the logarithmic geoclimatic factor $G$ and the duct occurrence probability, $P_d$ (%). An important aspect of these paths is that there are several in each vicinity, with more than one link in some cases (i.e., different frequencies and antenna heights), allowing average values of $G$ to be established for each region. Another is that duct occurrence statistics are available from radiosonde stations in the vicinities of each of these two groups of paths (Maniwaki, Que., and Prince George, B.C.). Finally, a third important point is that the two groups of paths represent close to the two extremes of most frequent and least frequent ducting occurrences that are possible over the Canadian land mass.

The average "observed" $G$ values obtained using the four-variable model of (16) for the Ottawa and Prince George areas are 5 dB and $-5$ dB, respectively. (The constant in (16) (viz. $-46$ dB) was adjusted to give an average of 0 dB between these two "extremes," but the 10 dB difference was coincidental.) The corresponding combined occurrences of surface and elevated-surface ducts in the worst-three-month periods are $P_d = 11.9\%$ for Maniwaki (Ottawa) and 2.5% for Prince George. Since the most plausible relationship between these two variables is a logarithmic one, as between $A$ and $P$, the transformation equation established from these two sets of values is

$$G = -10.9 + 14.8 \log P_d. \quad (25)$$

The "two-region fit" of (25) was used to establish the logarithmic geoclimatic factor map of Fig. 3. This map was then used to predict $G$ values for all the other experimental paths in question, and these are listed in Table 1.

**Discussion of fading measurements**

Several observations can be made from the data of Table 1 to aid in the prediction process. The presentation of both three- and four-variable calculations of $G$ demonstrates the importance of using the four-variable model (Method 2) wherever possible. The calculated fade depths based on the three-variable model (4) can differ by several decibels from those based on the four-variable model (16). There is a tendency for the three-variable model to underpredict the fade depth when the average path clearance is unusually large, and to overpredict when it is unusually small. It is for this reason that the average values of $G$ for the Ottawa and Prince George regions were determined using the four-variable model.

The use of $G$ values directly from the map of Fig. 3 for the over-water paths clearly results in an underprediction of the fading levels for these paths. This is not surprising since ducts are more prevalent over relatively large bodies of water such as those involved in the current data base. Moreover, it appears that, by and large, the Arctic paths that are over large bodies of water suffer from the greatest underprediction. It is interesting that the observed decreasing severity of the fading with distance northward on the UHF links in the Hudson Strait area [30] is consistent with this fact, since Frobisher Bay is considerably smaller and probably more subject to duct-inhibiting turbulence from surrounding mountainous terrain than Hudson Strait itself. This is the assumption that has been made in setting the two correction factors for over-water paths in Methods 1 and 2, these factors being chosen to give reasonable agreement with the admittedly small sample of data currently available for such paths in Table 1.

The "observed" $G$ values for the two groups of Arctic UHF paths (i.e., those in the vicinities of Hudson Strait and Viscount Melville Sound) are about 14 and 20 dB higher, on average, than the values predicted from the map of Fig. 3. This could be due entirely to the fact that the paths are all over water, but it is felt that differences in the diurnal patterns of duct occurrence in the Arctic and further south are more likely mostly responsible. For much of the year, the diurnal or nocturnal periods have much longer duration in the Arctic. It is therefore likely that ducts would persist for longer periods of time than is typical in the South. The statistical significance of a duct observation in the Arctic would thus be greater than that inferred from the observations at temperate latitudes.

A small part of the large difference between observed and predicted $G$ values in the Arctic could also be due to radiosonde resolution errors in measuring the occurrence of ducts, as noted earlier; ducts in the Far North tend to be somewhat thinner, on average, than those occurring at lower latitudes [29]. A small part could even be due to an error in the frequency extrapolation from SHF to UHF, although it should be quite small in view of the multifrequency results discussed previously. To be on the safe side for predictions above 60° latitude (i.e., approximately the latitude of the Hudson Strait measurements), a correction factor of 5 dB has been assumed for overland paths, and additional factors of 6 and 14 dB for paths over medium and large bodies of water, respectively.

One of the interesting and perhaps important results indicated by the data for both the Kemptville-Avonmore links and the links in the high Arctic is that deep fading appears to be less severe in some cases when path clearance is reduced. On the "near-grazing" Kemptville-Avonmore link, which has 0.6 Fresnel zone clearance [31], the improvement in the deep fading range of the distribution is 6.6 dB over the average of the other two links at 8 GHz with normal clearances. At UHF on the "grazing" Cockburn Lake-Lowther Peak link, the improvement is 13.4 dB over the Schomberg Peak-Cockburn Peak link, which has higher, but still less than 0.6 Fresnel zone, clearance. This is believed to be due to the fact that the direct wave for such links passes entirely below most ducts or else is launched from within the duct and suffers less loss due to beam spreading (defocussing) than if the duct were situated below the direct path [16]-[17]. In these particular examples, the effect appears to more than offset any tendency for the fading to be increased as a result of the smaller grazing angle involved, or as a result of earth diffraction during periods of subnormal refractivity gradients. However, it is important to note that the Lowther Peak-Martyr Peak link with its clearance of greater than 0.6 Fresnel zone still appears to show better performance (8.3 dB from the four-variable model) in deep fading conditions than the "grazing" Cockburn Lake-Lowther Peak link. (Note, however, that the original data for the latter path [32] do not clearly indicate the beginning of a tail, and the tail statistics in Table 1 may give larger observed values of $G$ than the actual values.) Thus, reducing path clearance does not necessarily lead to improved performance during multipath fading conditions.

The results for the high Arctic paths suggest, in fact, that there may be a clearance for which the fading is maximum. Maximum fading occurs on the Schomberg Peak-Cockburn Peak path with a minimum path clearance of about 55 m under normal conditions. This may have some relation to the fact that the mean thickness of surface ducts observed at Resolute was 61 m [29]. No such dependence of fading on path clearance (other than the effect of path clearance on grazing angle) has been observed for temperate climates [7], which may be due to a greater tendency for surface ducts to become elevated (or vice versa) as the solar elevation angle changes, or just to a lack of data for varying path clearance. Since there was some difference in the measurement periods for the high Arctic paths, the worst months for the two with the least fading occurring in 1983 and the worst months for the two with the most fading, in 1984, a degree of uncertainty remains. In any case, the result seems physically plausible, since fading would be reduced at low clearances for the reason noted above and at large clearances because of the combined lower occurrence of ducts and higher grazing angles. The likelihood that it may also occur in warmer climates needs further investigation. Some guidance on the setting of path clearance is given in a later section.

**Table 2**
**Summary of mean (*m*), standard deviation (*s*), and maximum (*max*) of prediction errors* (in dB) for various groupings of links**

| Link grouping | No. of links | Method 1 *m* | Method 1 *s* | Method 1 *max* | Method 2 *m* | Method 2 *s* | Method 2 *max* |
|---|---|---|---|---|---|---|---|
| All links | 33 | −0.1 | 5.5 | 16.4 | 0.1 | 5.0 | 12.2 |
| Reference** | 15 | 0.4 | 3.9 | 8.1 | 0.0 | 4.1 | 7.2 |
| Overland†, not including reference | 6 | 0.6 | 7.0 | 11.4 | −1.4 | 5.1 | 6.2 |
| Overland† | 21 | 0.5 | 4.8 | 11.4 | −0.4 | 4.3 | 7.2 |
| Southern† | 24 | 0.8 | 4.7 | 11.4 | −0.1 | 4.2 | 7.2 |
| Mountainous | 10 | 3.1 | 3.3 | 7.0 | −0.1 | 3.9 | 5.2 |
| Over-water | 11 | −1.2 (−8.6) | 7.1 (8.4) | 16.4 | 0.4 (−10.0) | 6.1 (7.8) | 12.2 |
| Arctic | 8 | −2.9 (−10.8) | 7.5 (8.7) | 16.4 | 0.1 (−11.9) | 7.0 (8.2) | 12.2 |

* Predicted minus observed values of $G$.
** Includes all links in Ottawa area (excluding Kemptville-Avonmore "near grazing" link).
† Excluding Kemptville-Avomore "near grazing" link.
Note: Means and standard deviations using uncorrected values of $G$ indicated in parentheses.

The fairly large variability in the observed geoclimatic factors for the Corkery-Shirley Bay and Kingsmere-Shirley Bay paths results from the very low percentage of time (0.001%) for the tail point on such short paths. Although the fading indicated for the Corkery-Shirley Bay path is worse at 11 GHz than at 17 GHz – the inverse of the result normally expected – no statistical significance should be attached to this result, since it was due to only a single eight-minute fading event that occurred at 11 GHz and not at 17 GHz. Nevertheless, the large number of links involved serves to improve the reliability of the average $G$ estimated for the Ottawa region.

### Limitations and accuracy of Methods 1 and 2

Estimated means, standard deviations and maxima of the prediction error for Methods 1 and 2 are given in Table 2 for different groups of data. These were obtained from the differences between the predicted and observed values of $G$ in Table 1. Results for the over-water and Arctic links are shown both with and without the correction factors for such links, those for the Arctic links, which are all over water, including both.

The first grouping of overland links outside the two reference regions (Ottawa and Prince George) was included because it gives some measure of how well the "two-region fit" applies to overland links in other temperate regions of the country. The grouping of all southern links does somewhat the same thing, but includes the results for the three over-water links which contain the 6 dB correction for links over medium-sized bodies of water. Comparisons with the results for all reference links suggest that the fit is indeed accurate for other temperate regions.

The grouping for mountainous links in British Columbia includes the five reference links in the Prince George area (nos. 12-16), those in the Salmo region (nos. 17-19), and those in the Hope region (nos. 20-21). The lower standard deviations for Method 1 with respect to Method 2, and for mountainous links with respect to all overland links, cannot be considered as statistically significant because of the small number of links involved. However, they do suggest that the predictions for mountainous links should be as accurate as, or at least not significantly less accurate than, predictions for links over flatter terrain.

The results for the grouping of over-water paths show the effect of the respective 6 and 14 dB corrections for medium-sized and large bodies of water. Since seven of these paths are in the Arctic, they also include the effect of the 5 dB correction for paths above 60° latitude. However, since the correction was derived from these results, they cannot be considered a true test of the accuracy of the over-water correction. Additional results for an independent set of over-water links would likely show larger errors, but these could then be used to improve the over-water correction. An obvious extension to the simple 6 and 14 dB over-water corrections is to use the suggested 10 dB correction factor in cases of uncertainty as to the size of the body of water.

The results for the Arctic links show the effect of the correction for links above 60° latitude and those for medium-sized and large bodies of water combined, since they are all over-water paths. Again, since the correction factors were based on the results themselves, the results cannot be considered as a true measure of the accuracy of Methods 1 and 2 in the Arctic. However, the fact that the mean error for the group of paths in the vicinity of Hudson Strait is close to that for the group in Viscount Melville Sound, and the fact that the uncorrected $G$ values for these two groups of paths based on the radiosonde data are almost identical, lend some confidence to the prediction for over-water paths in the Arctic. Since there are no results yet for overland Arctic paths, the 5 dB correction factor (which was based on the results for the three links in or at the entrance to Frobisher Bay (nos. 31-33) using the 6 dB correction for links over medium-sized bodies of water) remains to be fully tested.

A comparison of the standard deviations of error of 4.8 and 4.3 dB on overland links for Methods 1 and 2, respectively, with the corresponding values of 3.4 and 2.9 dB for the 47 overland links in France and the UK [7] might suggest that some accuracy has been lost in "transporting" the basic prediction equations to Canada. However, it must be remembered that the Canadian figures are all based on one-year worst-month fade depths, whereas the European figures are based on a mixture of one-year statistics and averages taken over two, three and four years. Such a mixture will inevitably reduce the standard deviation of error, since a finite but unknown component of the error is due to year-to-year statistical variability and not to intrinsic errors in the prediction equations. Furthermore, the proportion of unusual paths (i.e., very short or very rough) is larger in the Canadian data base. Considering that the predictions for six of the 21 overland paths are also based on geoclimatic factors scaled from refractivity gradient data, it is satisfying that the errors are as small as they are.

It must be emphasized that the small improvement in the standard deviations of error in Method 2 with respect to Method 1 does not adequately highlight the fact that the former method gives much greater accuracy for specific paths which have above- or below-average clearances. This is better shown by a comparison of the maximum errors for the two methods.

The British-French paths on which the model coefficients were based had an average clearance at midpath of 106 m (standard deviation of 70 m), and average clearance to dominant obstacles of 31 m under 4/3-earth refractivity conditions. Although the $\phi$ variable in Method 2 allows accuracy to be maintained over large clearance ranges, some inaccuracy is introduced when clearances are outside the range in the data base. This is seen in the results for the "near grazing" and "grazing" paths (nos. 11 and 29) discussed in the preceding section.

### Comparison with other methods

Three prediction methods particularly merit comparison with the new methods presented in this paper: the Bullington curves [6] sometimes used for the VHF and UHF bands; the Barnett-Vigants method [1]-[2] developed for the US, and used previously for paths in the SHF and upper UHF bands in Canada; and the version of the new methods for France and the UK [7].

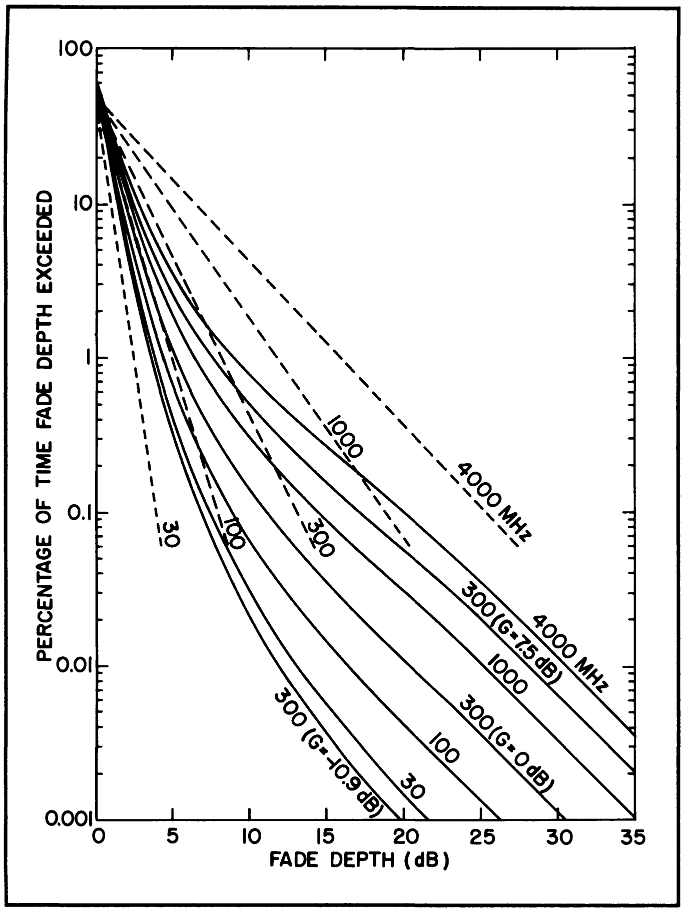


Figure 7: *Comparison of Bullington's curves (– – –) with results for Method 1 (——) for a 56 km (35 mi) horizontal path (results for Method 1 are for G = 0 dB, unless otherwise indicated at 300 MHz).*

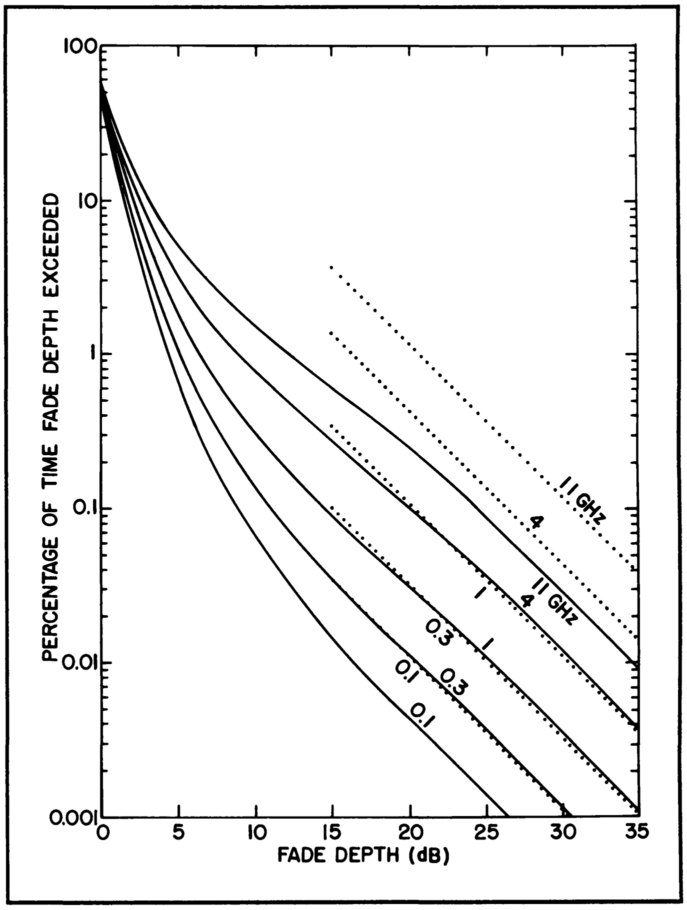


Figure 8: *Comparison of results for Barnett's method (· · · ·, C = 1) and Method 1 (——, G = 0) for a 56 km (35 mi) horizontal path in average fading conditions.*

A graphical comparison of the results of Method 1 (interpolation procedure for shallow fade depths) with the curves of Bullington is given in Fig. 7. For this comparison, a horizontal path ( $|\epsilon_p| = 0$) with a length of 56 km (35 mi) was assumed, corresponding to the average of the 30-40 mi range specified by Bullington. Curves are presented for five frequencies ranging from 30 MHz to 4 GHz for an assumed value of geoclimatic factor, $G = 0$ dB. For 300 MHz, curves are also given for the two most extreme values of $G$ below the 60th parallel, 7.5 dB and $-10.9$ dB, corresponding respectively to Port Erie, Ont. (Buffalo, N.Y.) and Fort Nelson, B.C.

The Bullington curves were based on experimental data, but unfortunately the author did not specify which data or frequency-dependence model were employed. Presumably some of the data used were those discussed in the section on extrapolation of the microwave tail models to VHF/UHF. One major limitation of the Bullington curves is that they show path variability only in terms of frequency. A less important limitation for the percentages of time typically of interest, is that they do not extend to the Rayleigh tail region.

It is perhaps a fortunate coincidence that the best agreement between the results of Method 1 (along with the interpolation procedure for shallow fade depths) and of Bullington occurs near 100 MHz, placing Bullington's curves on the conservative side for the 150 MHz and 450 MHz bands which have been used in Canada, at least under average fading conditions. Obviously Bullington's curves contain a larger frequency variability in the non-tail portion of the distribution, but with the limited data available, it is difficult to know which is the more accurate. However, it is important to note that the advantage of much greater path variability gained in the new methods (i.e., through the additional variables of geoclimatic factor, path length, path inclination and grazing angle) by far outweighs any possible loss of accuracy in the frequency dependence. This is illustrated in part by the curves in Fig. 7 for the "extreme" geoclimatic factors.

A graphical comparison of results from Method 1 and the method of Barnett [1] is given in Fig. 8, again for "average" climatic conditions in each case, and a path length of 56 km. The curves for Barnett's method are cut off at 15 dB, which is the limit of its applicability. Expressed in the same form as (4) and (16), the Barnett method is

$$A = 10 \log C - 42 + 30 \log d + 10 \log f - 10 \log P \quad (26)$$

for $d$ in km, $f$ in GHz, and $P$ in per cent. Here, $C$ is a factor that takes the value 1 for average climate and terrain conditions in the US, 4 for the Gulf of Mexico coast, and 1/4 for dry mountains, giving a variation in $10 \log C$ of $\pm 6$ dB. Vigants [2] extended the method by expressing $C$ in terms of surface roughness, which increased the total geoclimatic variability from 12 to 17 dB.

Some of the advantages of the new methods over those of Barnett and Vigants have already been discussed. Fig. 8 illustrates another: average fading conditions in the US, at least as expressed by the Barnett model, are more severe than in Canada. This is not surprising, in view of the greater likelihood of extreme refractivity gradients in the US [33]. However, some of the difference apparent in Fig. 8 disappears for longer paths because of the large coefficient for path length in Methods 1 and 2. The difference becomes greater for paths shorter than 56 km.

As noted previously, the constants in (4) and (16) were adjusted to give $G = 0$ for "average" fading conditions in Canada (i.e., midway between those for Ottawa and Prince George). In fact, the actual average value of $G$ for the 47 locations on the map of Fig. 3 (including the Arctic correction factor of 5 dB for the 16 locations above 60°N) is 0.1 dB.

The relationship between the logarithmic geoclimatic factor for France and the UK [7], here denoted by $G_E$, and that for Canada, is $G = G_E + 8$ (dB). This means that observed "average" fading conditions in France and the UK are more severe than those in Canada. This is partly due to the fact that few mountainous paths were included in the British-French data base. Indeed, an initial analysis of data for several paths in Switzerland [34] gives some very low values for the geoclimatic factor, similar to those in B.C. Another factor is that the average value of $G_E$ is further weighted towards high values by the extreme results from the East Anglia region of the UK [7], a region that appears to have more severe fading ($G_E = 8$ dB, or $G = 16$ dB) than even the Niagara peninsula region of Ontario.

### Implications for determining suitable path clearances

On the basis of the data for the Kemptville-Avonmore links and the earlier discussion, it is suggested that, in order to minimize tower heights and maximize link performance in multipath fading conditions, the antenna heights on the lower link in an SHF space-diversity configuration should be chosen, if possible, to give a 0.6 Fresnel zone path clearance from the terrain surface under 4/3-earth refractivity conditions (i.e., no diffraction loss). The upper link should still be designed to give a path clearance of at least that obtained from the design criteria for temperate climates cited in CCIR Report 338-6 [11]. To avoid increasing the height of existing towers, it would even seem appropriate to allow the lower link in a space-diversity configuration to graze the terrain surface in normal refractivity conditions, at least on paths with one or two isolated obstacles. The approximately 6 dB of extra diffraction loss (i.e., flat fading) incurred under normal refractivity conditions on a path having an obstacle approaching the shape of a "knife edge" would be well within link fade margins. The data for the Lowther Peak-Martyr Peak path in the Arctic would suggest that a grazing-clearance design for the lower link in a space-diversity configuration might be acceptable even for a relatively smooth path profile if the increased diffraction loss in both normal refractivity conditions (17 dB, for example, for the Lowther Peak-Martyr Peak path) and subrefractive conditions can be tolerated. A compromise solution would be to set the diversity antenna height to give a clearance of 0.3 Fresnel zone for either a path with one or two isolated obstacles or one in which the obstruction is extended along a portion of the path profile (i.e., a relatively smooth path). Again, the maximum 6 dB of extra diffraction loss incurred under normal refractivity conditions in the latter case [11] should be acceptable.

On the basis of the data for the links in Viscount Melville Sound, it is suggested that links in the 450 MHz band without diversity be designed for at least 0.6 Fresnel zone path clearance under 4/3-earth refractivity conditions. If tower costs are prohibitive, which might normally be the case unless they can be located on hilltops, it is suggested that grazing clearance under 4/3-earth refractivity conditions might be the next best alternative if fade margins are sufficiently large to make the increased diffraction loss under both 4/3-earth and subrefractive conditions acceptable. In a space-diversity configuration, it would certainly seem appropriate to design the lower link for grazing clearance of the terrain profile under 4/3-earth conditions as long as the increased diffraction loss in subrefractive conditions is acceptable. In the absence of other information, these procedures might also be used for other frequency bands in the upper VHF/UHF range of the spectrum.

The diffraction calculations required can be carried out using the computer program "PREDICT," resident at the Communications Research Centre.* In these calculations, the estimated value of the effective earth's radius factor, $k_{eff}(P\%)$, exceeded for $P$ per cent of the time (over a path of length $d$) that is necessary for estimating the diffraction loss exceeded for $100 - P$ per cent of the time can be obtained from

$$k_{eff}(P\%) = k(P\%) \quad d \leq 20 \text{ km}, \qquad (27.1)$$

$$k_{eff}(P\%) = k(P\%) + 0.53 \log(d/20) \quad 20 < d \leq 70 \text{ km}, \qquad (27.2)$$

$$k_{eff}(P\%) = k(P\%) + 0.29[1 + \log(d/70)] \quad 70 \text{ km} < d, \qquad (27.3)$$

where $k(P\%)$ is the point statistic estimated from the Tropospheric Refractivity Atlas for Canada [29]. Equations (27.1)-(27.3), which are based [35] on the curve for effective earth's radius versus path length given in CCIR Report 338-6 [11], are likely to be most accurate for exceedance percentages near 99.9%, but should be applicable over at least the range $99\% < P < 99.99\%$.

### Discussion and conclusions

Three new methods have been presented for predicting the average worst-month multipath fading distributions on VHF/UHF/SHF line-of-sight links in Canada. Method 1 does not require detailed path profile information and is best suited for preliminary planning or licensing purposes. Method 2 requires the path profile and should normally be employed in detailed link design. The interpolation procedure is used in combination with either Method 1 or 2 to predict the shallow fading range of the distributions. All methods make use of radioclimatological data on the map of Fig. 3. They have been presented in step-by-step form for ease of application.

These methods are considerably more accurate than the Barnett-Vigants and Bullington methods normally used previously in Canada for the SHF/upper UHF and VHF/UHF bands, respectively. This improved accuracy is mainly the result of four factors: the use of more statistically significant prediction variables; the use of one more prediction variable than the Barnett-Vigants method in the case of Method 2; the use of radioclimatological and propagation data specifically related to the Canadian environment; and the extrapolation of the accurate microwave models downwards in frequency.

Several improvements to the new methods are envisaged in the future. These include possible modifications to the basic tail models resulting from analysis of a larger data base [34] for several countries including Canada. Of particular importance would be inclusion of data for mountainous paths.

Further improvements to the radioclimatological statistics employed to determine geoclimatic variability may also be possible. These include the use of longer-term refractivity gradient statistics than the three-year statistics employed here, the use of average worst-month statistics rather than average worst-three-month statistics, and the use of statistics for gradients other than the ducting threshold. If more radio data become available for paths in the vicinity of radiosonde stations, improvement in the regression equation (25) relating the logarithmic geoclimatic factor $G$ to the refractivity gradient statistics may also be possible. Particularly lacking are suitable overland radio data for the Arctic from which to construct a more accurate Arctic correction factor, or preferably a new map with a more accurate relation between $G$ and refractivity gradient statistics as a function of latitude.

Similarly, improvements to the correction factor for over-water paths are envisaged once more over-water data become available. One approach to this problem is likely to be the pooling of data for more than one country at temperate latitudes. Extension of the interpolation method for shallow fade depths or development of a separate prediction technique for the enhancement range of the clear-air fading distribution would also be desirable, but is hampered by lack of data. Again, pooling of data for more than one country is likely to produce the quickest results.

* On-line access or purchase available from the Radio Propagation Directorate, Communications Research Centre, Department of Communications, P.O. Box 11490, Station H, Ottawa, Ont. K2H 8S2.

## Acknowledgements

The extrapolation of the basic microwave model to VHF/UHF was undertaken at the request of the DOC Spectrum Engineering section. The authors are grateful to Mr. Ted Devey for bringing this problem to their attention. Grateful thanks go to Mr. Mike Caskey of BNR for furnishing data and information on the Kemptville-Avonmore path, to Mr. Dwight Chang and Mr. Nev Owen of the B.C. Telephone Company for information on the paths in B.C., to Prof. Alan Webster of the University of Western Ontario (UWO) and Mr. Tim Merritt (formerly of UWO) for data and information on the Uniondale-London path, and to Mr. Claude Bilodeau of the Communications Research Centre (CRC) and Dr. Richard Butler (formerly of the CRC) for information on the Arctic paths. Thanks are also due to Dr. David Rogers, Dr. Jim Whitteker, and the three referees for their valuable suggestions in reviewing the manuscript. Finally, in the development of the basic microwave models, the first author would like to acknowledge the joint efforts of colleagues M. Louis Martin of the Centre National d'Études des Télécommunications (CNET) in France, and Mr. Terje Tjelta of Norwegian Telecom, and the helpful discussions with various CCIR colleagues. Much of this basic work was done while the first author was on an exchange visit to CNET in Lannion, France.

## References

[1] W.T. Barnett, "Multipath propagation at 4, 6, and 11 GHz," *Bell Syst. Tech. J.*, vol. 51, Feb. 1972, pp. 321-361.

[2] A. Vigants, "Space diversity engineering," *Bell Syst. Tech. J.*, vol. 54, Jan. 1975, pp. 103-142.

[3] N. Owen, B.C. Telephone Company Ltd., Vancouver, B.C., private communication, 1982.

[4] K. Morita, "Prediction of Rayleigh fading occurrence probability of line-of-sight microwave links," *Rev. Electr. Comm. Lab. (Japan)*, vol. 18, Nov.-Dec. 1970, pp. 810-821.

[5] N. Owen, E. Lee and M. Kharadly, "Analysis of microwave fading observations on certain microwave paths in British Columbia," in *Proc. URSI Commission F Symposium on Wave Propagation and Remote Sensing*, ESA Report SP-194, European Space Agency, Paris, France, April 1983, pp. 3-12.

[6] K. Bullington, "Radio propagation fundamentals," *Bell Syst. Tech. J.*, vol. 36, May 1957, pp. 593-626.

[7] T. Tjelta, R.L. Olsen and L. Martin, "Systematic development of new multi-variable techniques for predicting the distribution of multipath fading on terrestrial microwave links," *IEEE Trans. Antennas and Propagation*, vol. AP-38, Oct. 1990, pp. 1650-1665.

[8] L. Martin, R.L. Olsen and T. Tjelta, "Initial analyses of multipath fading measurements for various geographical conditions in France," in *Proc. Int. Symp. on Antennas and Propagation*, Kyoto, Japan, 1985, pp. 1067-1070.

[9] R.L. Olsen, T. Tjelta, L. Martin and J.E. Doble, "Towards a more accurate method of predicting the distribution of multipath fading on terrestrial microwave links," *Electron. Lett.*, vol. 22, Aug. 14, 1986, pp. 902-903.

[10] T. Tjelta, R.L. Olsen and L. Martin, "An investigation of terrain related variables for predicting the multipath fade depth distribution on terrestrial microwave links," in *Proc. NATO/AGARD Conf. on 'Terrestrial Propagation Characteristics in Modern Systems of Communication, Surveillance, Guidance and Control,'* Conf. Proc. No. CP-407, National Technical Information Service, Springfield, Va., Nov. 1987, pp. 1/1-9.

[11] CCIR Report 338-6, "Propagation data and prediction methods required for line-of-sight radio-relay systems," in *Proc. XVIIth Plenary Assembly, annex to vol. V*, International Telecommunication Union, Geneva, Switzerland, 1990, pp. 355-420.

[12] R.L. Olsen, T. Tjelta, L. Martin and B. Segal, "New worldwide techniques for predicting the multipath fading distribution on terrestrial line-of-sight links in the VHF/UHF/SHF bands," to be submitted for publication.

[13] L. Martin, "Une expression analytique pour la représentation de lois de probabilité théoriques et experimentales," Centre National d'Études des Télécommunications, Lannion, France, Note Technique NT/LAB/MER/314, 1988.

[14] R.L. Olsen, T. Tjelta and L. Martin, "Results of tests on a new method for predicting the distribution of multipath fading for various percentages of time," International Telecommunication Union, Geneva, Switzerland, CCIR IWP 5/2 Doc. 89/59, Apr. 3, 1989.

[15] N.R. Draper and H. Smith, *Applied Regression Analysis*. New York: John Wiley and Sons, 1981.

[16] R. Olsen, L. Martin and T. Tjelta, "A review of the role of surface reflection in multipath propagation over line-of-sight terrestrial microwave links," in *Proc. NATO/AGARD Conference on 'Terrestrial Propagation Characteristics in Modern Systems of Communications, Surveillance, Guidance and Control,'* Conf. Proc. No. CP-407, National Technical Information Service, Springfield, Va., Nov. 1987, pp. 2/1-23.

[17] R.L. Olsen, "The role of atmospheric stratification and surface effects in multipath propagation over terrestrial line-of-sight links: a review of some recent results," in *Proc. SBMO International Microwave Symp.*, Sao Paulo, Brazil, July 1989, pp. 401-408.

[18] T. Tjelta, R.L. Olsen and L. Martin, "Results of tests on methods for predicting the distribution of multipath fading at large fade depths," International Telecommunication Union, Geneva, Switzerland, CCIR IWP 5/2 Doc. 89/60, Apr. 27, 1989.

[19] M.P.M. Hall, "Activities in CCIR study group 5," *J. IERE*, vol. 58 (supplement), Sept.-Dec. 1988, pp. S244-S247.

[20] J.E. Doble, "Prediction of multipath delays and frequency selective fading on digital radio links in the U.K.," *IEE Colloqium Digest*, no. 62, 1979.

[21] L. Boithias, *Propagation des Ondes Radioélectriques*, Paris: Dunod, 1983, p. 139.

[22] CCIR Recommendation 581-1, "The concept of worst month," in *Proc. XVIth Plenary Assembly, vol. V*, International Telecommunication Union, Geneva, Switzerland, 1986, p. 230.

[23] K.W. Pearson, "Method for the prediction of the fading performance of a multisection microwave link," in *Proc. IEE*, vol. 112, July 1965, pp. 1291-1300.

[24] F. Carassa and P. Quarta, "Propagation tests at 250, 500, 1000, 2000 Mc/s on a 189 km path," in *Electromagnetic Wave Propagation*, M. Desirant and J.L. Michiels, Eds. London: Academic Press, 1960, pp. 471-478.

[25] F. Carassa, "Prove di propagazione con le frequenze di 250, 500, 1000 MHz," *Alta Frequenza*, vol. 25, May 1956, pp. 378-390.

[26] G.S. Wickizer and A.M. Braaten, "Propagation studies on 45.1, 474, and 2800 Megacycles within and beyond the horizon," in *Proc. IRE*, July 1947, pp. 670-680.

[27] A.L. Durkee, "Results of microwave propagation tests on a 40-mile overland path," in *Proc. IRE*, vol. 36, Feb. 1948, pp. 197-205.

[28] W. Klein and L.J. Libois, "Essais de transmission par faisceaux hertziens sur un long parcours en visibilité optique entre la France et la Suisse," *Onde Électr.*, vol. 33, 1953, pp. 665-677.

[29] B. Segal and R.E. Barrington, "The radio climatology of Canada: tropospheric refractivity atlas for Canada," Communications Research Centre, Department of Communications, Ottawa, Ont., CRC Report No. 1315, Dec. 1977.

[30] C. Bilodeau, "Measurements of UHF radio propagation on the Baffin and Labrador coasts," Communications Research Centre, Department of Communications, Ottawa, Ont., CRC Report No. 1430, July 1988.

[31] M. Caskey, Bell-Northern Research, Ottawa, Ont., private communication, 1987.

[32] R.S. Butler, "Measurements at 11 and 17 GHz of terrestrial microwave fading and depolarization," Communications Research Centre, Department of Communications, Ottawa, Ont., CRC Report No. 1358, Sep. 1982.

[33] B.R. Bean, B.A. Cahoon, C.A. Samson and G.D. Thayer, "A world atlas of radio refractivity," U.S. Department of Commerce, Washington, D.C., Monograph 1, 1966.

[34] CCIR Report 1144, "Data banks to support evaluation of prediction methods," in *Proc. XVIIth Plenary Assembly, annex to vol. V*, International Telecommunication Union, Geneva, Switzerland, 1990, pp. 1-25.

[35] CCIR Doc. 5/8, "Effects of refractivity on path clearance and on angle-of-arrival for line-of-sight radio-relay links," International Telecommunication Union, Geneva, Switzerland, Mar. 29, 1983.

[36] P.A. Kennard, J.D. McNicol and M.D. Caskey, "Fading dynamics in high spectral efficiency digital radio," in *Proc. IEEE Int. Conf. on Communications*, Toronto, Ont., 1986, pp. 1487-1492.

[37] T. Merritt, Centre for Radio Science, University of Western Ontario, London, Ont., private communication, 1987.

[38] W.I. Lam and A.R. Webster, "Microwave propagation on two line-of-sight oversea paths," *IEEE Trans. Antennas and Propagation*, vol. AP-33, May 1985, pp. 510-516.

[39] R.S. Butler, "The Northwest Passage propagation experiment: report of the 1983-1984 measurement program," Communications Research Centre, Department of Communications, Ottawa, Ont., CRC Report No. 1391, Sep. 1985.

[40] B. Segal, "Rain attenuation statistics for terrestrial microwave links in Canada," Communications Research Centre, Department of Communications, Ottawa, Ont., CRC Report No. 1351, Jan. 1982.